NeuroImage 218 (2020) 116924

Contents lists available at ScienceDirect

NeuroImage

journal homepage: www.elsevier.com/locate/neuroimage

Discovering dynamic task-modulated functional networks with specific spectral modes using MEG

Yongjie Zhu [a,b,c], Jia Liu [a,b], Chaoxiong Ye [f,g], Klaus Mathiak [c], Piia Astikainen [g], Tapani Ristaniemi [b], Fengyu Cong [a,b,d,e,*]

[a] School of Biomedical Engineering, Faculty of Electronic and Electrical Engineering, Dalian University of Technology, 116024, Dalian, China
[b] Faculty of Information Technology, University of Jyväskylä, 40014, Jyväskylä, Finland
[c] Department of Psychiatry, Psychotherapy and Psychosomatics, Medical Faculty, RWTH Aachen University, Pauwelsstraße 30, D-52074, Aachen, Germany
[d] School of Artificial Intelligence, Faculty of Electronic Information and Electrical Engineering, Dalian University of Technology, Dalian, China
[e] Key Laboratory of Integrated Circuit and Biomedical Electronic System, Liaoning Province. Dalian University of Technology, Dalian, China
[f] Institute of Brain and Psychological Sciences, Sichuan Normal University, Chengdu, 610000, China
[g] Department of Psychology, University of Jyväskylä, 40014, Jyväskylä, Finland

ARTICLE INFO

Keywords:
Tensor decomposition
MEG
Functional connectivity
Frequency-specific oscillations
Dynamic brain networks
Canonical polyadic decomposition

ABSTRACT

Efficient neuronal communication between brain regions through oscillatory synchronization at certain frequencies is necessary for cognition. Such synchronized networks are transient and dynamic, established on the timescale of milliseconds in order to support ongoing cognitive operations. However, few studies characterizing dynamic electrophysiological brain networks have simultaneously accounted for temporal non-stationarity, spectral structure, and spatial properties. Here, we propose an analysis framework for characterizing the large-scale phase-coupling network dynamics during task performance using *magnetoencephalography* (MEG). We exploit the high spatiotemporal resolution of MEG to measure time-frequency dynamics of connectivity between parcellated brain regions, yielding data in tensor format. We then use a *tensor component analysis* (TCA)-based procedure to identify the spatio-temporal-spectral modes of covariation among separate regions in the human brain. We validate our pipeline using MEG data recorded during a hand movement task, extracting a transient motor network with beta-dominant spectral mode, which is significantly modulated by the movement task. Next, we apply the proposed pipeline to explore brain networks that support cognitive operations during a working memory task. The derived results demonstrate the temporal formation and dissolution of multiple phase-coupled networks with specific spectral modes, which are associated with face recognition, vision, and movement. The proposed pipeline can characterize the spectro-temporal dynamics of functional connectivity in the brain on the subsecond timescale, commensurate with that of cognitive performance.

1. Introduction

The brain is composed of billions of interconnected neurons, forming an extremely complex dynamic system in which populations of neurons are organized into functional units with specific information-processing capabilities (Babiloni et al., 2005; Hillebrand et al., 2012). Yet, efficient neuronal coordination between these spatially separated units is necessary for cognitive functions (Salinas and Sejnowski, 2001; Siegel et al., 2012; Varela et al., 2001). The interactions among distributed regions through oscillatory synchronization may provide a possible mechanism of such coordination (Fries, 2005, 2015). In other words, neuronal populations transmit information by coordinating their oscillatory activity with the oscillations of the receptor population at certain frequencies (Vidaurre et al., 2018). Moreover, different oscillatory patterns (i.e., different frequencies) provide the basis for different functions (Buzsáki and Draguhn, 2004; Vidaurre et al., 2018). Meanwhile, phase-coupling between separate populations of neurons in specific frequency rhythms has been well-established as a mechanism for regulating the integration and flow of cognitive contents (Engel et al., 2013; Salinas and Sejnowski, 2001; Vidaurre et al., 2018). It has also been shown that such frequency-specific phase-coupling plays an important role in task performance, in which task-related information is transmitted through

* Corresponding author. School of Biomedical Engineering, Faculty of Electronic and Electrical Engineering, Dalian University of Technology, 116024, Dalian, China.
E-mail addresses: yongjie.zhu@foxmail.com (Y. Zhu), cong@dlut.edu.cn (F. Cong).

https://doi.org/10.1016/j.neuroimage.2020.116924
Received 28 October 2019; Received in revised form 31 March 2020; Accepted 4 May 2020
Available online 20 May 2020

phase-locking across spatially distributed cortical regions (Bola and Sabel, 2015; Fries, 2015).

Magnetoencephalography (MEG) recordings have demonstrated that large-scale networks activated in cognitive tasks involve different frequency bands in their communications. For instance, the connectivity between the left and the right motor regions, quantified by the correlation of band-limited power, is maximized in the beta band (13–30 Hz), but not significant at low frequencies (1–8 Hz) or high frequency (i.e. >40 Hz) (Brookes et al., 2012a,b; Brookes et al., 2014; Brookes et al., 2012a,b; Hipp et al., 2012). Moreover, certain frequency bands are related to distinct cognitions. For example, electrophysiological studies of working memory have shown that power and coherence in the beta band decrease with increased memory load in the frontoparietal network. However, the power in theta the band only increases in the frontal regions, while the power in the alpha band exhibits a reduction with increased task load in the parietal nodes (Brookes et al., 2012a,b; Brookes et al., 2014). These findings imply that connectivity patterns at distinct frequency bands may subserve different cognitive functions.

In addition to specificity in spectral features, functional networks exhibit highly temporally variable neuronal dynamics on rapid timescales (Bola and Sabel, 2015; Kopell et al., 2014). In order to effectively track such network dynamics, many studies have explored the organization of brain functional networks using MEG, since the temporal richness of MEG can match the rapid timescales of the brain's functional connectivity (O'Neill et al., 2017; Schölvinck et al., 2013; Tewarie et al., 2019b). For example, Vidaurre and colleagues have published multiple papers using a set of methods based on the *Hidden Markov Model*, showing that functional brain networks reorganize and coordinate transiently on the timescale of milliseconds (Baker et al., 2014; Quinn et al., 2018; Vidaurre et al., 2018; Vidaurre et al., 2017). O'Neill et al. proposed an *independent component analysis* (ICA)-based method for time-varying functional connectivity, demonstrating the temporal evolution of dynamic networks at a specific frequency band on the timescale of seconds during a task (O'Neill et al., 2017). Lachaux and colleagues presented a practical method based on phase-locking for the direct quantification of frequency-specific synchronization with time resolution at the millisecond scale (J. P. Lachaux, Rodriguez, Martinerie and Varela, 1999; Varela et al., 2001). Also, the brain networks are recently understood as a multi-scale network and can be characterized over temporal scales with precision ranging from sub-millisecond to that of the entire lifespan (Betzel and Bassett, 2017; Betzel et al., 2016; Khambhati et al., 2019).

Considering the temporal non-stationarity and frequency specificity of the functional connectivity, previously applied methods typically required pre-specification of a frequency band and/or a time window before connectivity calculation. Those methods need to filter the neuroimaging data into specific frequency bands and examine the temporal dynamics of interactions for one specific frequency band by one (de Pasquale et al., 2012; de Pasquale et al., 2016). For examples, Betti et al. linked the dynamics of formation and dissolution of networks and of hub networks during movie observation to the one occurring during resting stage using a fixed frequency band (Betti et al., 2018; Betti et al., 2013). O'Neill et al. provided an overview of the studies on the dynamics of connectivity carried out with fixed frequency intervals but without pre-specification of the time window (O'Neill et al., 2018; O'Neill et al., 2015). However, the above-mentioned methods were reliant on a priori selection of frequency bands, and few studies have attempted to explore the formation and dissolution of the frequency-dependent dynamic brain networks during task performance within a completely data-driven approach.

In the current study, we undertake an analysis of the spectral features and temporal evolution of dynamic connectivity during a task. Our proposed framework is based on the measurement of the time-frequency domain connectivity between pairs of separate brain regions predefined through cortical parcellation. *Weighted phase lag index* (wPLI) is used as a means of quantifying the connectivity since it is insensitive to signal leakage and similar bias effects (Hillebrand et al., 2012; Palva et al., 2018; Vinck et al., 2011). After calculation of the wPLI for each time point and frequency point, we construct a *third-order tensor* (a three-dimensional data array) including frequency, time, and connectivity (vectorized upper triangular parts of the connectivity matrix). The three-dimensional data is then analyzed using *tensor component analysis* (TCA), which is a multi-dimensional decomposition technique and is an extension of matrix factorization (e.g., principal component analysis (PCA) or ICA). TCA can extract separate components with low-dimensional features (factors), each of which corresponds to a functional connectivity pattern with rapidly temporal dynamics and distinct spectral dynamics. It should be noted that unlike PCA or ICA, the factors extracted by tensor decomposition do not require orthogonality or independence. According to this property, tensor decomposition can achieve a demixing of high-dimensional data and examine the interaction across different modalities (Zhou and Cichocki, 2012; Zhou et al., 2016). For example, in an EEG study, three tensor modes could correspond to time, frequency, and channel (Mørup et al., 2006). In fMRI studies, the different modes could be voxel, time, and patient (Hunyadi et al., 2017). In neurophysiological measurements, they could span neuron, time, and trial (Williams et al., 2018). Previous TCA-based studies of brain connectivity mainly applied TCA to channel-level EEG data to detect the change points of the dynamic network states (Liu et al., 2014; Mahyari and Aviyente, 2014; Mahyari et al., 2016; Samdin et al., 2016) and examine the spatial-temporal properties of the network community (Al-sharoa, Al-khassaweneh, & Aviyente, 2018; Ozdemir et al., 2017; Tang et al., 2019). Also, TCA was applied to EEG channel level connectivity over time, frequency and subjects to explore the connectivity patterns within the considered electrodes (Pester et al., 2015), and to ongoing EEG data over temporal sliding windows, frequency, and subjects to link musical features to brain networks (Zhu et al., 2019a,b). Here distinct from this, we applied TCA to atlas-based MEG data over network connectivity, time and frequency to provide a pipeline to track the temporal evolution of frequency-dependent functional networks at the millisecond scale during task performance. We performed tensor decomposition to extract three interacted, low-dimensional descriptions of time-frequency phase-coupling networks, which includes connectivity factors reflecting functional network patterns, temporal factors reflecting rapidly temporal evolution of the functional networks, and the spectral factors reflecting spectral features of networks. The proposed pipeline is completely data-driven and enables the characterization of the temporal, spectral, and spatial features of the electrophysiological network connectivity all at once. In other words, this allows us to identify which involved frequency bands, where and when significant modulations in connectivity occur.

2. Material and methods

2.1. Data description

We analyzed MEG data from the human connectome project (HCP; www.humanconnectome.org), including a motor task and an N-back working memory task (Larson-Prior et al., 2013). Sixty-two subjects participated in the motor task and 82 subjects in the working memory task. Most were right-handed as measured with the Edinburgh Handedness Inventory, with a mean lateralization quotient of 65% and $SD = 44\%$ (Oldfield, 1971). Data were recorded using a whole-head 248-channel magnetometer system (MAGNES 3600 WH, 4D Neuroimaging, San Diego, CA) with the participants in supine position. Data were continuously recorded with a sampling rate of 2034.5 Hz and a bandwidth of DC-400 Hz. Digitization of the participants' head shape and of the locations of the fiducial coils was accomplished with a Polhemus 3Space Fasttrak system. Participants performed a sequence of tasks, described in detail in the reference manual provided by HCP. Just prior to the N-back working memory task the participant underwent three runs of approximately 6 min of resting-state MEG recording.

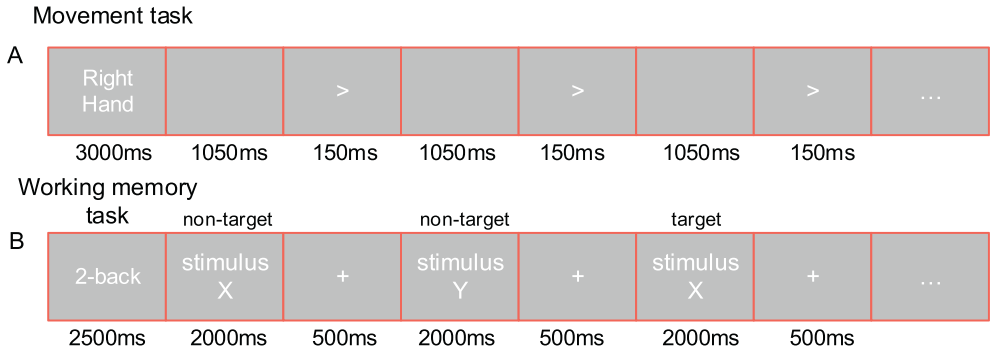

Fig. 1. Experiment task. A) Right hand movements in motor task paradigm. Block begins with a 3 s cue instructing the participant which limb to move in that trial. B) Two-back condition in the working memory task. Two-back blocks were signaled by a presentation of "2-back" for 2500 ms. Participants indicated whether the presented stimulus matched the stimulus two trials earlier.

During the motor task, participants were presented with visual cues instructing the movement of either the right hand, left hand, right foot, or left foot. Movements were paced with a visual cue, which was presented in a blocked design. Each block started with an instruction screen, indicating the limb (arm or leg) and the side to be involved in the current block. A set of pacing stimuli were presented in sequence, each one instructing the subject to make a brisk movement. The pacing stimulus was composed of a small arrow in the center of the screen (see Fig. 1). The interval between consecutive stimuli was fixed to 1200 ms. The arrow stayed on the screen for 150 ms and the screen was black for the remaining 1050 ms. There were 8 blocks of movement per motor effector. 10 pacing stimuli were presented in sequence. This yielded in total of 80 movements per motor effector. Here, for simplicity, we only used data with right- and left-hand movements.

During the N-back working memory task, subjects were presented with pictures of tools or faces. There were two memory load conditions: 0-back and 2-back tasks. 0-back task is a match-to-sample condition during which a cue target image was presented at the beginning of a block. A set of images were presented in a sequence, and each of them was displayed for 2000 ms. At the end of this interval, a button press had to be executed by participants with the index or middle finger of the right hand as to whether this current image matched the target or not. For the 2-back condition block, participants were presented with a sequence of images and had to respond whether each image matched the image two positions earlier or not. The response had to take place within a 500-ms period after stimulus presentation, during which a fixation cross was presented on the center of the screen. Participants were presented with 8 blocks in the 2-back condition. A sequence of 10 images is presented in each block. This yielded in total number of 80 trials.

2.2. Preprocessing and source reconstruction

We used the same criteria set in the HCP pipelines to remove bad channels, segments and bad independent components.[1] Briefly, epochs had been extracted from the continuous recording. Epochs containing superconducting quantum interference device (SQUID) jumps, bad sensors, or bad segments, defined as excessive signal amplitude changes $> \sim 10^{-12}T$, were excluded from further processing. Eye movement-related signals and cardiac signals had been identified with ICA and projected out of the data. For the motor task, trial duration was set from −1.2 to 1.2 s relative to the onset of the arrow that instructs subjects to execute the movement. For the working memory task, trial duration was set from −1.5 to 2.5 s relative to the onset of the image that subjects had to match or not with the target image. After bandpass filtering (1–48 Hz), the data were down-sampled to 256 Hz. Following this preprocessing, the cortical surface of the brain was reconstructed from an anatomical individual MRI offered by HCP. The reconstructed cortical surface was decimated to 4098 evenly distributed vertices per hemisphere. The preprocessed data epochs were used to compute the inverse model, which was estimated using cortically constrained and depth-weighted (p = 0.8) L2 minimum-norm estimate (wMNE) (Lin et al., 2006). The noise covariance matrix was calculated from the empty-room recordings, separately for each subject's data provided by HCP. The cortical surface was then parcellated into 68 anatomical regions based on the Desikan-Killiany Atlas (Desikan et al., 2006). This atlas discretized the neocortex into 34 parcels (areas) per hemisphere. For each parcel, we performed a principal component analysis to extract spatially orthogonal components that describe the activity, ordered by amount of variance explained. We selected the first principal component as a representation of the parcel's time course of activity. Thus, for each trial, a source-level data matrix M was created with dimension $n_n \times n_s$, where $n_n = 68$ represented the number of anatomical regions and n_s represented the number of samples ($n_s = 615$ for the motor task, $n_s = 1024$ for the working memory task). The main steps of the subsequent data processing pipeline are outlined in Fig. 2.

[1] https://www.humanconnectome.org/documentation/MEG/MEG1_Release_Reference_Manual.pdf.

2.3. Spectral decomposition

To estimate the spectral densities of the parcellated time-series data, continuous wavelet transform with Complex Morlet wavelets was performed on source space data matrix M for a single trial. A total of 42 linearly spaced frequencies and full time points were estimated. The wavelet contained three cycles at the lowest frequency (4 Hz); the number of cycles increased up to 15 cycles at the highest frequency (45 Hz), and 42 frequency points from 4 Hz to 45 Hz were obtained. Thus, for each trial, a third-order tensor was obtained with dimension $n_n \times n_s \times n_f$, where $n_f = 42$ represented the number of frequency points.

2.4. Functional connectivity estimation

To estimate phase-coupling between all pairs of regions for each frequency and time point, wPLI (Vinck et al., 2011) was computed; i.e., the sign of the phase difference between two signals is weighted by the magnitude of the imaginary component of the cross-spectrum:

$$wPLI_{(f,t)} = \frac{\left|\sum_{n=1}^{N}\left(\left|im\left(S_1^n(f,t)S_2^{n*}(f,t)\right)\right| sign\left(im\left(S_1^n(f,t)S_2^{n*}(f,t)\right)\right)\right)\right|}{\sum_{n=1}^{N}\left|im\left(S_1^n(f,t)S_2^{n*}(f,t)\right)\right|}, \quad (1)$$

where $S_1^n(f,t)$ and $S_2^n(f,t)$ are wavelet-decomposed time-frequency representations from regions 1 and region 2 respectively, from trial n and for frequency point f and time point t. N is the number of trials. * represents the complex conjugate, $im()$ is the imaginary part of a complex value, and $||$ represents an absolute value operation. For each subject, a third-order tensor of connections $\mathcal{P}$ was created with dimension $n_c \times n_s \times n_f$, where

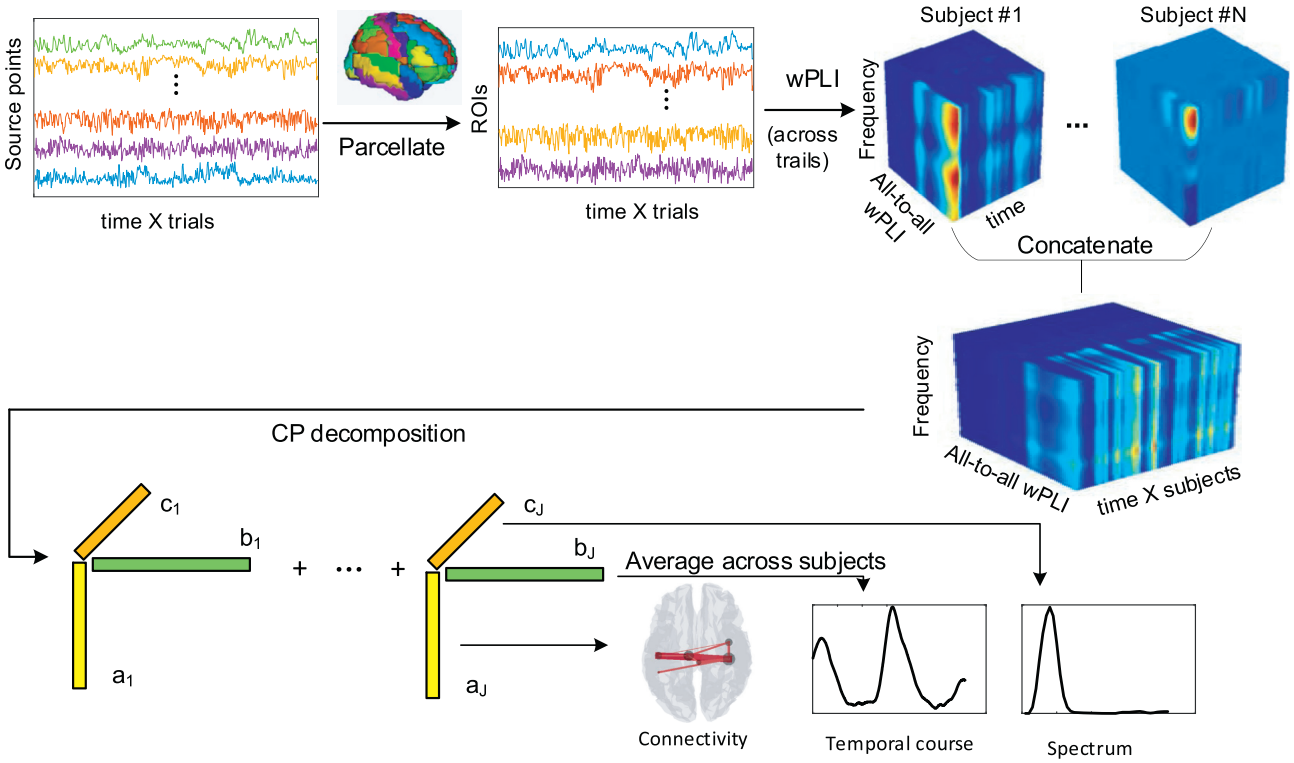

Fig. 2. Analysis pipeline. Data were preprocessed, divided into stimulus-locked epochs, and projected into the source-space using the weighted MNE algorithm. Signals of 68 ROIs based on anatomical brain regions were transformed with a Complex Morlet wavelet. For each time-point and frequency-point, an adjacency matrix containing wPLI estimates was then generated (vectorized using upper triangular parts). For each subject, a three-way tensor (with time by frequency by connection) was obtained. These individual wPLI (average across trails) tensors were concatenated across subjects in temporal dimension. Nonnegative CANDECOMP/PARAFAC (CP) decomposition was performed on the temporally concatenated tensor to extracted low-dimensional components including temporal factors, spectral factors, and connectivity factors.

$n_c = 2278$ denotes the number of pairs of regions $(68*(68-1)/2)$. These three-way arrays were then concatenated over time to generate a new tensor $\mathcal{X}$ with dimension $n_c \times n_t \times n_f$, where $n_t = n_s * n_p$ and n_p denotes the number of the participants ($n_p = 61$ for the motor task and $n_p = 83$ for the working memory task).

2.5. Tensor decomposition

The most common method for dimensionality reduction and component analysis of electrophysiological data has been based on decomposition techniques such as PCA and ICA. However, these two-way analysis techniques commonly applied on matrices may fail to find the underlying structures in multi-dimensional data sets (Cong et al., 2012; Williams et al., 2018). Here, we use the CANDECOMP/PARAFAC (CP) model (Sidiropoulos et al., 2017), a direct extension of bilinear factor models to multilinear data, to identify a set of low-dimensional components characterizing variability along each of the modalities. A brief description of the CP model follows.

Each element in the obtained tensor $\mathcal{X} \in \mathbb{R}_{+}^{n_c \times n_t \times n_f}$, $x_{c,f,t}$ denotes the connection (wPLI) between two regions at time point t within frequency bin f. Here, the indices c, t, and f each range from 1 to n_c, n_s, and n_f, respectively. It should be noted that all the elements are non-negative, since wPLI takes values between 0 and 1. CP decomposition approximates the data as a sum of outer products of three vectors producing an additional set of low-dimensional factors, which can be described as:

$$\mathcal{X} \approx \sum_{j=1}^{J} \boldsymbol{a}_j \circ \boldsymbol{b}_j \circ \boldsymbol{c}_j, \tag{2}$$

where operator $\circ$ represents the outer product of vectors, and J is the number of extracted components. $\boldsymbol{a}_j, \boldsymbol{b}_j$, and $\boldsymbol{c}_j$ $(n = 1, 2, \cdots, J)$ are the factor vectors. We can think of $\boldsymbol{a}_j$ as the functional network pattern across the whole-brain connections, and we can consider $\boldsymbol{b}_j$ as spectral factors across frequency. These connectivity factors and spectral factors constitute a structure that is common across time. The third set of factors, $\boldsymbol{c}_j$, can be considered as temporal factors, which characterizes the temporal evolution of the frequency-specific functional connectivity patterns identified by connection and spectral factors. Thus, TCA for wPLI data can capture temporal dynamics of the functional connectivity on a timescale of milliseconds with a specific spectral feature. Such frequency-specific connectivity patterns may be modulated by a task across time during task performance. In addition, another benefit of TCA is a dimension reduction of the original high-dimensional data, reducing $n_c \times n_s \times n_f$ data points to $J(n_c + n_s + n_f)$ elements.

The non-negative CP model optimization is to solve the following minimization problem:

$$\min_{\boldsymbol{A},\boldsymbol{B},\boldsymbol{C}} \frac{1}{2} \left| \mathcal{X} - \sum_{j=1}^{J} \boldsymbol{a}_j \circ \boldsymbol{b}_j \circ \boldsymbol{c}_j \right|_F^2, \tag{3}$$

where $_F$ represents the Frobenius norm. Matrix $\boldsymbol{A} = [\boldsymbol{a}_1, \ \boldsymbol{a}_2, \cdots, \boldsymbol{a}_j]$ is the connectivity factor matrix, $\boldsymbol{B} = [\boldsymbol{b}_1, \boldsymbol{b}_2, \cdots, \boldsymbol{b}_j]$ is spectral factor matrix, and $\boldsymbol{C} = [\boldsymbol{c}_1, \boldsymbol{c}_2, \cdots, \boldsymbol{c}_j]$ is temporal factor matrix. Like many matrix factorization methods, the CP model can only be fit by iterative optimization algorithms. Such procedures may converge in suboptimal local minima, but in other applications, all estimations for many runs have converged to similar reconstruction errors (Cong et al., 2012; Mackevicius et al., 2019; Williams et al., 2018). For example, Williams et al. applied the TCA to neural data to extract low-dimensional neural dynamics across multiple timescales, where the majority of runs for optimization successfully converged with high data fit value (Williams et al.,

2018). In the current study, we apply the classic method of *alternating least-squares* (ALS) to estimate the factor matrices (Cichocki et al., 2015; Kolda and Bader, 2009). To solve the minimization problem in Equation (3), the ALS algorithm fixes two of the factor matrices and optimizes over the third one. This is a least-squares subproblem that is convex and has a closed-form solution. For illustration, consider estimating the connectivity factor matrices $\boldsymbol{A}$, while fixing the spectral factor matrices $\boldsymbol{B}$ and temporal factor matrices $\boldsymbol{C}$. This yields in the following updating rule:

$$\boldsymbol{A} \leftarrow \operatorname{argmin}_{A} \frac{1}{2}\left|\mathcal{X} - \sum_{j=1}^{J} \boldsymbol{a}_j \circ \boldsymbol{b}_j \circ \boldsymbol{c}_j\right|_F^2, \tag{4}$$

which can be estimated as a linear least-squares problem. We terminated the CP decomposition process when the absolute difference value of data fitting of the adjacent two iterations was less than very small positive value such as $1e-8$, or the maximum number of iterations was more than 1000. Here, TCA was performed on temporally concatenated data across subjects. This means that the connectivity factor and the spectral factor of the brain networks (components) are common to all subjects but the temporal factor is subject-dependent. Each subject has their own temporal courses, representing the time evolution of the frequency-specific networks at each time points. The ALS algorithm is available in several open-source toolboxes (Bader and Kolda, 2012; Vervliet et al., 2016).

2.6. Selection of component number

In the application of tensor decomposition, a crucial issue is the determination of the number of components to be extracted. Actually, the choice of the number of components to extract is an inherent problem of model order selection, which is usually for the linear transform model or other dimensionality reduction methods (Cong et al., 2012, 2013; Mørup and Hansen, 2009). Although many different methods have been developed in the past few years, there does not exist a perfect solution for all conditions. Here, we used the DIFFIT method as a reference to inform this choice. DIFFIT refers to the difference in data fitting, and is calculated based on model reconstruction error and the explained variance (Timmerman and Kiers, 2000; Wang et al., 2018). The reconstruction error of the CP model is defined as

$$ReErr(J) = \frac{\left|\mathcal{X} - \sum_{j=1}^{J} \boldsymbol{a}_j \circ \boldsymbol{b}_j \circ \boldsymbol{c}_j\right|_F}{|\mathcal{X}|_F}. \tag{5}$$

Reconstruction error provides a metric analogous to the fraction of unexplained variance often used in PCA, since it is normalized to range between 0 and 1. Let the number of components $J \in [1, \mathscr{J}]$, where $\mathscr{J}$ is the empirically maximal number of underlying components. A fit is the variance of raw data explained by a proposed model and can be obtained as

$$Fit(J) = 1 - ReErr(J) = 1 - \frac{\left|\mathcal{X} - \sum_{j=1}^{J} \boldsymbol{a}_j \circ \boldsymbol{b}_j \circ \boldsymbol{c}_j\right|_F}{|\mathcal{X}|_F}. \tag{6}$$

Unlike PCA, the optimization procedure of tensor decomposition may have suboptimal solutions (local minima), and there is no guarantee that optimization routines will find the best set of parameters for decomposition. Thus, we run the optimization algorithm underlying the CP model at each value of J 20 times from random initial conditions, and the average data fitting $\overline{Fit(J)}$ is calculated across many runs. Then, the difference fit of the two adjacent fits is

$$DIF(J) = \overline{Fit(J)} - \overline{Fit(J-1)}. \tag{7}$$

Next, the ratio of the adjacent difference fits reads as

$$DIFFIT(J) = \frac{DIF(J)}{DIF(J+1)}. \tag{8}$$

The model $\tilde{J}$ with the largest DIFFIT value is considered as the appropriate tensor factorization model for the raw data tensor.

2.7. Testing the task-modulation connectivity

The above analyses yielded a set of $\tilde{J}$ brain networks (TCA components) with distinct spectral features, temporal courses, and connectivity patterns. Here, we sought to determine which extracted components were significantly modulated by the tasks. It should be noted that our procedure was based on previously theory, which has been well described elsewhere (O'Neill et al., 2017; Winkler et al., 2014; Zhu et al., 2019a,b). We first averaged the temporal factor matrix $\boldsymbol{C}$ (with a dimension of $n_s n_p \times \tilde{J}$) across subjects, yielding a new temporal matrix $\overline{\boldsymbol{C}}$ (with a dimension of $n_s \times \tilde{J}$) containing $\tilde{J}$ subject-averaged temporal courses. After this, an empirical null distribution was constructed based on phase randomization (Brookes et al., 2014).

We defined a "sham" matrix, $\tilde{\boldsymbol{C}}_{\text{onset}}$, which was constructed in exactly the same way as $\overline{\boldsymbol{C}}$, but prior to averaging over subjects, the onset of individual temporal courses was randomly shuffled based on phase-randomization. The phase-randomization was computed by taking the Fourier transform, randomizing the phase angle, and then transforming back. The properties of the derived time series of each individual subject were exactly preserved in the spectral domain. We reasoned that if no task induced response was expected, the randomly shuffled onset times would be meaningless, and therefore the magnitudes of fluctuations in $\tilde{\boldsymbol{C}}_{\text{onset}}$ and $\overline{\boldsymbol{C}}$ would match. However, if the individual temporal courses contained time-locked responses in brain connectivity, which were robust over subjects, then these would be preserved in $\overline{\boldsymbol{C}}$ but diminished in $\tilde{\boldsymbol{C}}_{\text{onset}}$. This procedure was repeated 5000 times to generate an empirical null distribution for each extracted component.

A component was considered significant if, at any one time point in the subject average, the corresponding column of $\overline{\boldsymbol{C}}$ fluctuated such that it fell outside a threshold defined by the null distribution (randomized onset). The threshold for significance was defined at level $P < 0.05$. This significant level was corrected based on Bonferroni correction for multiple comparisons across the multiple ($\tilde{J}$) components. In addition, a two-tailed distribution was allowed since the magnitude of the average temporal courses could be either greater than, or less than the null distribution. Thus, the threshold for significance was set at $P_{corrct} < 0.05/(2 \times \tilde{J}) = 0.025/\tilde{J}$.

3. Results

In the following section, we show the flexibility of our framework in the real MEG dataset. However, our proposed framework was also validated in simulation and compared with permutation test procedure without TCA (see Supplementary material). These simulation results can be found in the Appendix.

We firstly ran CP at each value of J—linearly increasing from 1 to 40 ($\mathscr{J} = 40$)—20 times with random initial conditions, which enabled us to examine whether some runs converged to local minima with low data fitting value (or high reconstruction error). Fig. 3 demonstrates the averaged fit values (Fig. 3A), the difference of fit values (DIF) and the DIFFIT (Fig. 3B). As can be seen that the variance (shaded areas of Fig. 3A) of the fit values from the 20 times is very low, and reveals that all runs at fixed component number J yield the same data fitting. For the motor task, it can be seen that the DIF values become very close to 0 when the component number $J > 20$ and a local maximum on DIFFIT at $J = 20$ emerges. This suggests the data fitting value starts to converge, which can be also found from the data fitting curve. The data fitting curve also reveals that all runs at fixed J yield similar results, indicating that all local minima in the optimization process are similar to each other and thus are

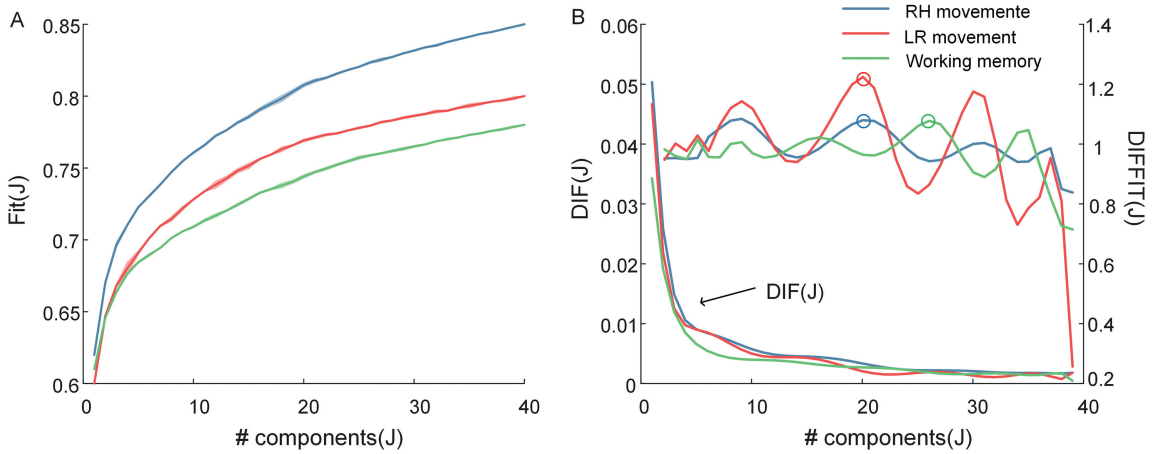

Fig. 3. A) Fit value plotted against number of components. B) difference of fit values and the DIFFIT plotted against number of components. For the movement experiments, we chose 20 components decomposed by the CP model. For the working memory task, 25 components were extracted since the delta fit was relatively small. It should be noted that the results were robust when the number of components was set from 15 to 25.

presumably similar to the global minimum. Fig. 3B demonstrates that $J = 25$ may be the appropriate model for CP decomposition in the working memory task since the DIF values are close to 0 after $J = 25$. Hereinafter, we set $\tilde{J} = 20$ for the motor task and $\tilde{J} = 25$ for the working memory task. Note that the DIFFIT method just gives a reference to select the number of underlying components, and we discuss this further below.

Fig. 4 demonstrates the results of the proposed approach performed on the movement data. While $\tilde{J} = 20$ rank-1 components were extracted, here we presented only two brain network patterns that exhibited significant task modulation. The other brain networks are shown in the Supplementary material. In Fig. 4, the right side shows the results of the left-hand movement data and the left side shows the results of the right-hand movement data. Each row of Fig. 4 represents a component with three factors. Fig. 4A demonstrates the connectivity factor representing the brain network pattern, which is demonstrated in 3D visualization and thresholded (top 5%) for clarity. Fig. 4B shows the temporal factor reflecting the time evolution of this network, which is represented as the associated averaged temporal factor of the individual in $\overline{\boldsymbol{C}}$ (with a dimension of $n_s \times \tilde{J}$) and plotted by black line. The time line of the event is marked by the vertical line. The gray shaded area indicates the null distribution constructed by randomly shuffling the time onset ($\tilde{\boldsymbol{C}}_{\text{onset}}$), which is the 95th percentile threshold. Fig. 4C shows the spectral factor reflecting the oscillatory feature of this network. A network shown in Row I, representing primary somatosensory and motor regions, is modulated significantly by the left-hand movement task (Fig. 4B). It is also found in right-hand movement data depicted in Row III. It should be noted that the results are slightly different for different sides of the hand movements. The 3D visualization demonstrates that network connectivity is mainly located in the left primary somatosensory cortex for right-hand movement (Row I of Fig. 4A), and on the right primary somatosensory cortex for the left-hand movement (Row III of Fig. 4A). Fig. 4C in Rows I and III show the spectral features of the sensorimotor network modulated by the movement task. It can be clearly seen that the sensorimotor network is associated with frequency modes ranging from 15 to 30 Hz, corresponding to the classical beta band. Rows II and IV show another visual network, modulated significantly by visual cues. The spectral feature suggests that this visual network is related to the theta and alpha bands. This spectra-specific visual network is derived from both left- and right-hand movement tasks.

Fig. 5 demonstrates the results of our analysis pipeline applied to the 2-back working memory data. Obviously, the increased cognitive load induced by 2-back working memory tasks elicits alterations in a large

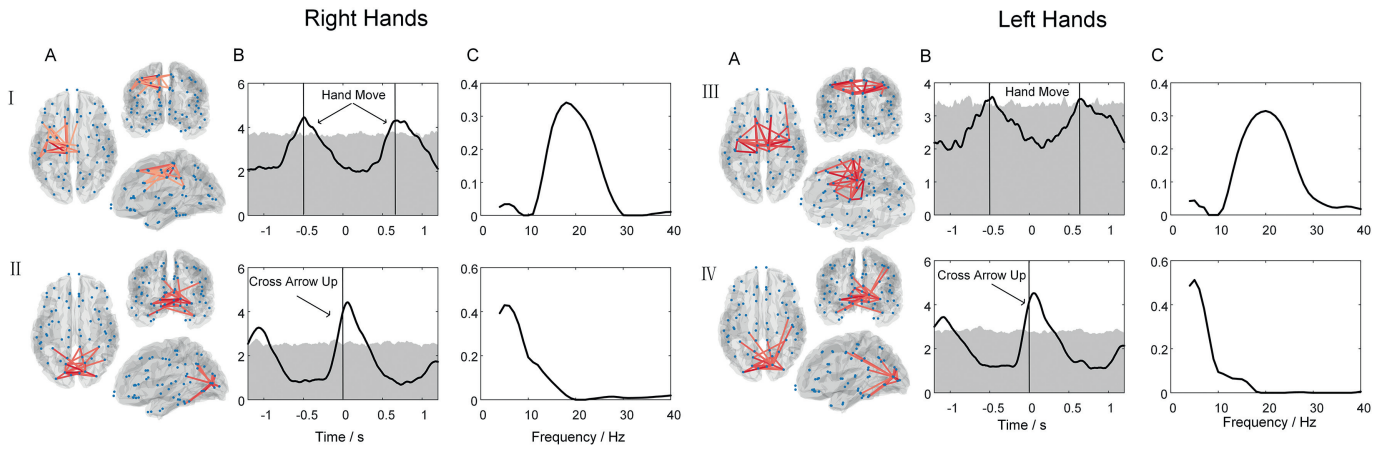

Fig. 4. Results of the hand movement experiments. The left side shows the results of the right hands' movement, and the right side shows the results of the left hands' movement. The separate columns show A) 3D representation of connectivity factors, thresholded (top 5%) for visualization. Each node indicates one brain region and darker color of lines shows stronger connections. B) The temporal courses of the network patterns during finger movement task, averaged across subject (black line). The gray shaded region represents the null distribution based on the hypothesis that the response is not time-locked to the stimulus. C). The spectral mode of the network. Rows I and III show the beta oscillatory motor networks modulated significantly by movement task. Rows II and IV show the theta oscillatory visual networks modulated significantly by the presentation of cross arrows.

number of functional networks. We present 10 of the 25 brain networks extracted that exhibited significant modulation by the 2-back working memory task. Each row in the column indicates one component with three factors, including connectivity networks represented as 3D visualization (Fig. 5A), temporal evolution represented as averaged time courses across subjects alongside a null distribution based on randomly shuffled time onset (Fig. 5B), and spectral features (Fig. 5C).

Two primary visual networks shown in Rows II and III of Fig. 5 are significantly modulated by the figure stimuli, which is unsurprising in light of the visual nature of the task. Their connectivity magnitudes increase by around 200 ms after both presentation and disappearance of the figure stimuli, but the connectivity during presentation increases more than during disappearance of the stimuli. Although these two networks both involve the visual regions, their spectral features are different. The spectral mode of network II peaks around 5 Hz, spanning theta and low alpha bands, but the spectral mode of network III peaks around 13 Hz across high alpha and low beta bands. Row IX, with spectrum peaking at 10 Hz, demonstrates connections between the primary visual and parietal regions, showing an increase in connectivity around 150 ms after the presentation of the figure stimuli. Row I shows a right-lateralized connection between visual and temporal areas with a spectral mode spanning the alpha band, which exhibits a significant enhancement immediately during the appearance of the stimuli. Rows IV to X show that transient functional networks with distinct spectral features form in later task phases. Row IV shows an increase in connectivity between right frontal areas and temporal areas related to the theta band, around, 300 ms after presentation of the stimuli. Row X indicates that a connection between left frontal regions and right temporal regions emerges by 300 ms after the stimuli, with a spectral feature across theta and alpha bands. A high-alpha right-lateralized tempo-parietal network appearing around 400 ms after the stimuli is shown in Row VII. Row VI shows a bilateral temporal connectivity network with dominated alpha rhythm, emerging at 600 ms after the stimuli. The network also captures areas associated with semantic processing and is thus termed the *semantic network*. Row VIII highlights a left-lateralized network that incorporates regions of temporal, parietal, and frontal cortex. The regions implicated are strongly associated with the production of language as well as shape and pattern recognition. A beta sensorimotor network is also derived during feedback. Row V demonstrates that a sensorimotor network involved in beta rhythm emerges during the execution of the button press. The connection exhibits strong enhancement in left motor areas, since participants executed the button press with their right-hand. In addition, the significant increases span a large range, from 1200 ms to 2000 ms, since the timing of the button press was different for different subjects. This result is in line with the results of the motor task (Fig. 3). It is worth noting that the brain areas involved in these networks incorporate the primary sensory cortices, association areas, and cognitive networks that would be associated with semantic processing, face recognition, and verbalization, and so these networks are plausible given the task. These are further addressed in our discussion.

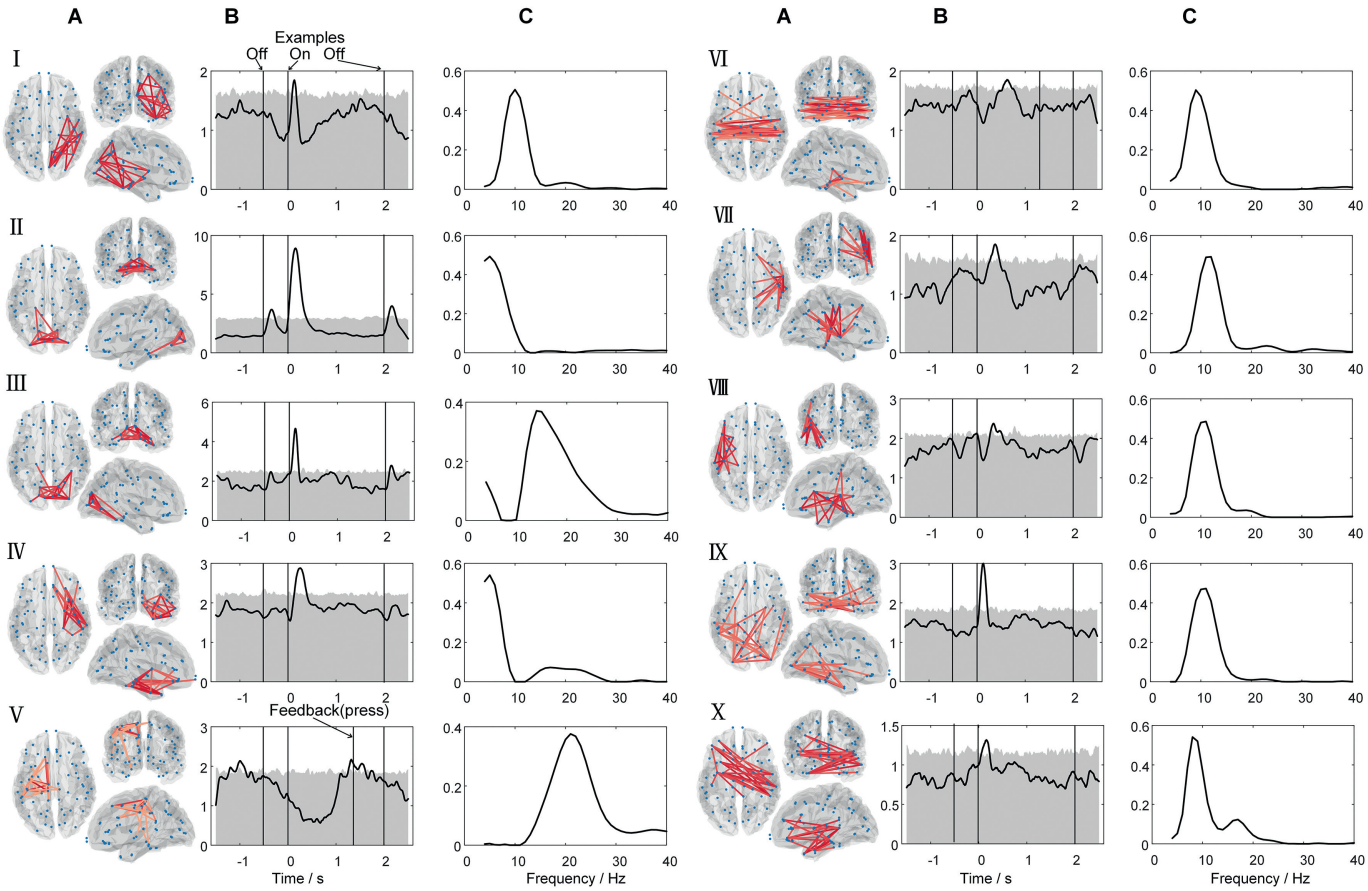

Fig. 5. Results of 2-back working memory task. A) 3D network visualization. B) Average temporal course (black line) and null distribution based on randomized onset times (shaded areas). C) Spectral mode of the network patterns. Row I: right lateralized connections between visual and temporal areas with a spectral mode spanning alpha band. Rows II and III: primary visual networks with theta and high-alpha dominant spectrum. IV: connections between right frontal areas and temporal areas related to theta band. V: Beta-specific motor network. VI: a bilateral temporal connectivity network with dominated alpha rhythm. VII: alpha-dependent right lateralized temporo-parietal network. VIII: language-related network. IX: visual to parietal with alpha-dominant spectrum. X: connections between left frontal regions and right temporal regions.

4. Discussion

The present study introduced a tensor-based framework for deriving large-scale phase-coupled network dynamics with distinct spectral features. This pipeline allows characterization of transient reconfiguration of electrophysiological brain networks at the timescale of milliseconds when applied to MEG data. Previous methods typically required prespecification of a frequency band and/or a time window around the stimuli onset before the connectivity calculation. Then, network dynamics were examined using matrix decomposition techniques, such as ICA and PCA, in a single frequency band. Compared with ICA-based approaches, the TCA-based framework is completely data-driven and enables the characterization of the temporal, spectral, and spatial features of the electrophysiological network connectivity all at once. Tensor decomposition can provide dimension reduction for big data and extract three interacted, low-dimensional patterns representing the high dimensional time-frequency coupling data. Here, we calculated time-frequency domain phase-coupled functional connectivity quantified by wPLI and applied TCA to extract three interacted, low-dimensional descriptions, including a connectivity factor reflecting spatial network pattern, a temporal factor reflecting rapidly temporal evolution of the functional networks, and a spectral factor reflecting frequency modes of networks. By doing so, we identified the temporal dynamics of phase-coupled networks with specific spectral modes, in a completely data-driven way. This enabled us to identify where, when, and in which frequency band significant modulations in connectivity occur. We validated our proposed framework in a simulation (see Appendix) and a simple movement task compared with the permutation test procedure without TCA (see Supplementary material). Furthermore, we demonstrated the utility of our pipeline applied to a complex cognitive task and showed that frequency-specific functional networks transiently form and dissolve to allow participants to complete a 2-back working memory task.

Tensor analysis methods have been well investigated from a theoretical perspective (Cichocki et al., 2015; Kolda and Bader, 2009; Sidiropoulos et al., 2017; Zhou et al., 2015), and applied to a variety of neuroimaging data (Cong et al., 2015; Spyrou et al., 2019; Williams et al., 2018; Zhu et al., 2019a,b). Some studies have applied tensor factorization to sensor-level EEG data and fMRI data most typically to examine differences between subjects in extracted multi-features (Cong et al., 2012, 2013; Kanatsoulis et al., 2019), rather than across functional connectivity. Some recent studies have examined the temporal evolution of functional networks based on TCA across adjacency matrix, subjects, and time, but did not investigate the spectral features, and only studied channel-level EEG connectivity rather than source-reconstructed MEG connectivity networks (Spyrou et al., 2019; Tang et al., 2019). Although TCA was also applied to EEG channel level connectivity over time, frequency and subjects to explore the connectivity patterns within the considered electrodes (Pester et al., 2015), and to ongoing EEG data over temporal sliding windows, frequency, and subjects to link musical features to brain networks (Zhu et al., 2019a,b), we here applied TCA to atlas-based source-level MEG data over network connectivity, time and frequency to explore the formation and dissolution of frequency-dependent functional networks during task performance. The introduced MEG-TCA-network pipeline is able to reliably determine spectral-specific functional networks since functional connectivity is calculated for a set of atlas-based ROIs in anatomical space that covers almost the entire brain, aiding the interpretation of MEG functional network studies, as well as the comparison with other modalities (e.g. fMRI). By establishing a novel link between tensor analysis and frequency specific networks, we found that analysis of the extracted factors can directly identify spatial patterns of functional connectivity with distinct spectral modes as well as reveal temporal dynamics on the timescale of milliseconds.

It should be noted that the temporal courses of the functional networks shown in Figs. 4 and 5 indicate a decrease and increase in connectivity. That is, the peaks refer to the time points when two or more brain areas defining a network are most phase-synchronized. Just because regions involved in networks are not synchronized at particular time points does not mean that these regions are not engaged in the task. This is an important point, as many areas involved in networks are likely to be engaged continuously over the working memory task. In addition, our pipeline has an excellent temporal resolution since we calculated the connectivity at each time point. Fig. 4 demonstrates that a beta-dependent network of brain connections involving primary somatosensory and motor cortices, as well as supplementary motor regions, was successfully identified based upon the finger movement task, which is in agreement with the ICA-based study (O'Neill et al., 2017). This sensorimotor network was modulated significantly by the finger movement. In contrast to the motor areas, which engaged in both movements due to contralateral effects, network connectivity is centered on the right primary somatosensory cortex for left-hand movement (Row I of Fig. 4A), and on the left primary somatosensory cortex for right-hand movement (Row III of Fig. 4A). Another difference of the motor connectivity between right- and left-hand movement is the greater variability in time course of the connectivity across subjects during left-hand movements, since the non-dominant hand was used for the majority of participants. Furthermore, a primary visual network with spectral modes across the theta and alpha bands, modulated by visual cues, was also derived by our pipeline in both left- and right-hand movement. The beta and alpha oscillations engaged in the visual networks were observed. Accumulating evidence has shown that information is sampled periodically at low frequencies (theta: 4–7 Hz and alpha: 8–12 Hz). Specifically, the alpha and theta rhythms seem to coexist in the brain and support different functions (Dugué and VanRullen, 2017; Dugué et al., 2017). If alpha has been related to an ongoing, sensory rhythm, theta appears related to attentional exploration of the visual space (Senoussi et al., 2019). This theta-specific primary visual network was not obvious in the ICA-based study (O'Neill et al., 2017), where the data were filtered into beta bands (13–30 Hz) before calculating connectivity. Thus, the ICA-based study failed to derive the visual network during the movement task (O'Neill et al., 2017). We also validated our pipeline by comparing one of the results from the hand movement (see Fig. S1), with the permutation test procedure (Maris and Oostenveld, 2007). These results validate our proposed pipeline by identifying the sensorimotor connectivity with enhanced beta frequency modes, modulated by movements, and a theta-specific visual network modulated significantly by visual cues.

In the working memory task, the formation of networks including visual and sensorimotor regions with distinct spectral modes is consistent with the presentation of visual stimuli and execution of the motor response (O'Neill et al., 2017; Woodward et al., 2013; Yamashita et al., 2015). A modulation in the theta band was also observed. Numerous studies demonstrated that human theta can be engaged in the working-memory task and the synchronized theta oscillations might be coordinated by working-memory task (Raghavachari et al., 2006). Nodes in the occipital lobe typically include the lateral fusiform gyrus which is specialized for perception of faces (Dima et al., 2018; Elbich et al., 2019). Networks of connectivity from the posterior superior temporal sulcus to both the right occipital face area and the right fusiform face area, with specific beta modes, emerged during the presentation of the face examples, which is in line with a recent study (Elbich et al., 2019). Other frequency-specific networks encompass brain regions that are considered to be important for the higher-order cognition needed for successful completion of the working memory task. Enhanced alpha (8–14 Hz) activity in broad brain areas, including the dorsolateral prefrontal cortex (DLPFC), parietal and occipital regions, and superior temporal cortices, is particularly evident in the majority of these networks. Many studies of the neural oscillatory dynamics serving working memory processing have implicated broad alpha rhythm activity in these brain areas as being essential for task performance (Embury et al., 2019; Heinrichs-Graham and Wilson, 2015). Particularly, the right DLPFC is recruited in network IV connection with the right superior temporal sulcus, which is mainly involved in theta frequency activity. Network VI also shows that the

DLPFC is connecting bilaterally with the inferior superior temporal sulcus in alpha frequency domain. It has been shown that the alpha oscillations in the left and right DLPFC, widely known to play a cognitive and attentional control function in working memory (Barbey et al., 2013; O'Neill et al., 2017), synchronize temporally as a function of time during decoding, maintenance, and retrieval phases (Heinrichs-Graham and Wilson, 2015). Network VI incorporates bilateral inferior temporal gyri regions considered important for semantic processing, which has been referred to as a semantic network (O'Neill et al., 2017). This alpha-specific network was also observed in a previous study, in which the connectivity between the DLPFC and ventral visual regions varied with cognitive load in a working memory task (Barbey et al., 2013; O'Neill et al., 2017; Popov et al., 2018). Another cognitive network VIII with spectral mode peaking in 10 Hz was also identified and termed the language network by other researchers (O'Neill et al., 2017). According to previous studies, working memory is more efficient for social information than for nonsocial information (Thornton and Conway, 2013). Participants could use the strategy of chunking or verbal labeling to enhance working memory performance for social information. Indeed, this left-lateralized network is anchored in the angular gyrus with extensions to the inferior frontal gyrus, inferior temporal gyrus, and a number of nodes spanning the inferior to superior precentral gyrus. These regions are consistent with previous accounts of semantic cognition (O'Neill et al., 2017). Overall, the transient frequency-specific networks elicited by 2-back working memory task are plausible given the previous studies on working memory and sensory processes.

The proposed analysis framework can identify the spectral, temporal, and spatial patterns of the electrophysiological networks that are transient form and dissolve during task performance. In doing so, several key points should be considered while interpreting the results generated by our pipeline. It should be noted that there is significant variability in the temporal courses of frequency-specific connectivity across subjects since temporal resolution is on the timescale of milliseconds; this variance is exhibited in the average time courses across subjects. For example, the low-level visual network is highly synchronized across subjects during the presentation of the image example. Thus, the individual temporal change of this visual network was similar and did not jitter in all subjects, which was demonstrated by the fact that the peak of the average time course would be far greater than the null distributions (gray shaded areas) and the duration of the above null distributions would be very short (thin curve; see Fig. 4 II). The time courses of motor network time-locked button presses fluctuated across subjects; thus, the duration of the above null distributions of the time courses would be long, showing the time-locked temporal change jittered across subjects (see Fig. 4 III). Although relatively poor between-subject reproducibility of MEG connectivity measurements has been demonstrated (Colclough et al., 2016; Wens et al., 2014), our framework still allows detection of the quasi-time-locked temporal change in frequency-specific networks using large cohorts during task performance. In addition, we perform tensor factorization on the time-concatenated three-way tensor form, where the underlying spatial connectivity patterns and the frequency mode are common to all subjects while each subject has its own temporal courses. Then the individual time courses were averaged across subjects to identify components modulated by task. This less-relaxed assumption could discard some components possibly involved in the task due to the inter-subject differences. In other words, the task-modulated temporal patterns of some components would be diminished due to inter-subject variability of the task-induced response. For example, in the movement task, some networks involving the somatomotor cortex with alpha dominant spectrum (see. Fig. S5 IV, XI and XII) show modulations of connectivity which seem to be related to the stimulus despite the temporal courses below the threshold. Future work should therefore seek other strategies to not only consider the inter-subject synchronization but also the inter-subject variability. Actually, this assumption for MEG connectivity study has also been introduced in previous studies (O'Neill et al., 2017; Vidaurre et al., 2018). For example, O'Neill et al. applied ICA to the time-concatenated adjacency matrix calculated by the envelope correlation to character temporal dynamics of networks (O'Neill et al., 2017), where all subjects share common spatial connectivity patterns but have different temporal courses. In fact, the connectivity within several well-known distributed networks is stable even though their temporal variability is significant across subjects. However, the temporal courses of connectivity networks may be similar among subjects when performing the same repeated task. An alternative method is to apply tensor decomposition to a fourth-order tensor with time, frequency, connection, and subject modes, to examine the specificity of subjects (Pester et al., 2015). This will be one of our future study directions.

In addition, we here used the wPLI (phase-based method) as a means of quantifying the connectivity. Since phase reflects the timing of population-level activity, it can be conceptualized as a "functional configuration" or a "functional state" (Cohen, 2014). However, the phase-coupling-based methods might be non-sensitive to the induced synchronization (e.g. beta event-related synchronization in post-movement). The envelopes of band limited oscillations metrics have been proved to detect fluctuations of connectivity during the well-known post-movement beta rebound (Seedat et al., 2020; Tewarie et al., 2019a; Vidaurre et al., 2016). Another limitation is that we only considered the low-frequency coupling (1–48Hz). There is enough evidence that the high frequency rhythms are important to understand transient coherent functioning in the brain in other fields as epilepsy or vision (Jensen et al., 2007; J.-P. Lachaux, Axmacher, Mormann, Halgren and Crone, 2012; J.-P. Lachaux et al., 2005). However, we here only considered the width-band signal since we assume no prior knowledge about which frequency bands are dominant. This would result in failing to extract the high-frequency coupling by tensor decomposition since the low-frequency signal were dominate in the working memory task. It would be better to examine the high-frequency coupling by tensor decomposition separately for those researchers who are interested in the high-frequency activity.

Another consideration in the application of tensor decomposition is the selection of the number of components. Choosing the number of components is not a limitation of our algorithm directly, but rather is a challenging and fundamental problem for all tensor-based methodologies. In this study, we performed an empirical study using a range of numbers of components for tensor models and applied the DIFFIT method to determine the optimal number of components. In addition, we also tried other numbers, showing that varying this parameter in our current work made little difference to the overall results. It should also be noted that the components were retained based on the fact that their temporal dynamics were modulated significantly by the task. However, if a network does not show significant modulation with the task, it does not simply mean that this network is not genuinely representative of connectivity. If the current pipeline is applied for a resting-state study, other techniques should be considered to validate the extracted networks.

5. Conclusion

The characterization of electrophysiological brain networks based on the phase synchronization of spatially separate brain regions, which are transient and dynamic on the timescale of milliseconds, in order to support specific cognitive tasks, is one of the important challenges in cognitive neuroscience. In this paper, we propose a TCA-based pipeline to describe temporal, spectral, and spatial signatures of such dynamic brain networks using MEG data. We applied CP decomposition to a third-order tensor formed by time-frequency domain phase-coupled connectivity, to extract three interacted, low-dimensional descriptions of connectivity data, including a connectivity factor reflecting spatial pattern, a temporal factor reflecting rapidly temporal evolution of the functional networks, and a spectral factor reflecting frequency modes of networks. The proposed framework allows us to identify the temporal dynamics of phase-coupled networks in specific spectral modes in a completely data-driven way. We validated our pipeline in a simulation and a simple

motor task, successfully identifying a beta-specific sensorimotor network during finger movement and a theta-specific visual network modulated by visual cues. We also used the proposed pipeline with a relatively complex task (2-back working memory task) showing transient reconfiguration of electrophysiological brain networks on the timescale of milliseconds. These findings demonstrate that the proposed framework seems valuable in the characterization of electrophysiological brain network connectivity.

Data and code availability

The data used in the manuscript are from the human connectome project (HCP; www.humanconnectome.org). The analysis code will be found in the first author' website soon.

Declaration of competing interest

None of the authors have potential conflicts of interest to be disclosed.

CRediT authorship contribution statement

Yongjie Zhu: Conceptualization, Data curation, Formal analysis, Investigation, Methodology, Visualization, Writing - original draft, Writing - review & editing. **Jia Liu:** Data curation, Formal analysis, Methodology, Writing - review & editing. **Chaoxiong Ye:** Writing - review & editing. **Klaus Mathiak:** Methodology, Writing - review & editing. **Piia Astikainen:** Writing - review & editing. **Tapani Ristaniemi:** Supervision, Conceptualization, Writing - review & editing. **Fengyu Cong:** Supervision, Conceptualization, Funding acquisition, Project administration, Resources, Writing - review & editing.

Acknowledgment

This work was supported by the National Natural Science Foundation of China (Grant No. 91748105&81471742), the Fundamental Research Funds for the Central Universities [DUT2019] in Dalian University of Technology in China, and the scholarship from China Scholarship Council (No. 201600090042; No. 201600090044). Y. Zhu was also supported by the Mobility Grant from the University of Jyvaskyla. We would like to thank the anonymous reviewers for constructive suggestions and comments.

Appendix A. Supplementary data

Supplementary data to this article can be found online at https://doi.org/10.1016/j.neuroimage.2020.116924.

Appendix. Validation by simulation

The validation of our proposed pipeline provided in this manuscript focuses on its application to real MEG dataset. However, our pipeline also has been validated by simulation data. The performance of the wPLI as a measure of connectivity in source level has been addressed well in previous publications (Palva et al., 2018), and we will not examine its performance repeatedly here. However, the ability of tensor factorization (CP decomposition in this paper), applied to connectivity in a time-frequency domain, to explore the temporal, spectral and spatial features of functional networks has not been tested. In the current study, we validated the ability of tensor factorization by performing CP decomposition on a third-order tensor formed by a set of simulated brain networks.

Simulation methods

We firstly used the outer product of three predefined factors, temporal, spectral, and connection factors, to generate a simulated adjacency tensor $\mathcal{Q}_{sim}$ as the ground true connectivity networks. A noise (bandwidth:1–48 Hz) tensor $\mathcal{N}_{sim}$ with same dimensions was added to form a synthetic adjacency tensor $\mathcal{P}_{sim}$. It can be represented by

$$\mathcal{P}_{sim} = \mathcal{Q}_{sim} + \quad \mathcal{N}_{sim} = \sum_{j=1}^{J} \boldsymbol{a}_{sim}^{j} \circ \boldsymbol{b}_{sim}^{j} \circ \boldsymbol{c}_{sim}^{j} + \mathcal{N}_{sim}$$

where $\boldsymbol{a}_{sim}^{j}$, $\boldsymbol{b}_{sim}^{j}$ and $\boldsymbol{c}_{sim}^{j}$ represented connectivity factor, spectral factor and temporal factor of the j-th component. Here, three spatially distinct connectivity patterns were constructed based on a previous study (O'Neill et al., 2017). The spatial factors of connectivity, including visual, sensorimotor, and fronto-parietal networks, were separately represented by an adjacency matrix (see Fig. A1). Their temporal and spectral signatures were demonstrated in Fig. A1. The temporal factors were constructed by 4000 ms of Hanning windows. We set the amplitude to unit length 1, and the full width half maximum to 200 ms, and their onsets were set to 150, 300, and 500 ms. The spectral factors were constructed by filtering white noise with bandwidth centered at 5 Hz, 12 Hz, and 20 Hz. The outer product of temporal factors, spectral factors, and connectivity factors (vectorized adjacency matrices) was performed to adjacency tensor $\mathcal{Q}_{sim}$. The noise tensor $\mathcal{N}_{sim}$ was constructed by source reconstructing recorded empty room MEG data (also provided by HCP) onto a simulated brain geometry. The wPLI was calculated based on the methods described in this paper. Noise tensor $\mathcal{N}_{sim}$ effectively represented connectivity networks of interest.

In order to test the ability of tensor analysis to extract interpretable descriptions including spectral, temporal, and spatial connectivity signatures of brain networks under noise, we tested the performance in the presence of different noise-levels and defined a similarity merit to characterize how well a single component with their three factors represented the simulated temporal, spectral, and spatial connectivity of a network. We also tested the impact of selection of the frequency on the separation in simulation. The bandwidth of noise varies from 1 Hz to B ($B \in [30,\ 100\ Hz]$) with fixed SNR = 0 dB.

Temporal similarity: For each component, we calculated the correlation coefficients between its temporal factor and all the true time courses of the three simulated networks. We thought of the maximum correlation coefficient as the best-matching simulated networks. The temporal similarity was defined as the mean of maximum correlation across all the components.

Spectral similarity: Similar to temporal similarity, we calculated the correlation coefficients between the spectral factor of each component and all the true spectrum of the three simulated networks. The max correlation coefficient was considered as the best matching simulated networks. The

spectral similarity was defined as the mean of this maximum correlation across all the components.

Connected similarity: We also calculated the correlation coefficients between connect factor of each component and all the true adjacency matrices of the three simulated networks. The max correlation coefficient was considered as the best-matching simulated networks. The connected similarity was defined as the mean of this maximum correlation across all the components.

Simulation results

Fig. A1 demonstrates the temporal, spectral, connectivity factors of simulated and reconstructed networks. To test the performance of the CP decomposition, we ran this analysis 20 times under different noise levels, between −35 dB and 25 dB in steps of 2 dB, and calculated the mean of temporal, spectral and connected similarity across runs with varying the signal to noise ratio (SNR) of the simulated data. As expected, the figure of similarity was high at high SNR, meaning that our simulated networks are reconstructed successfully (Fig. A2B). However, a sharp transition below a minimum threshold SNR was observed, at which the similarity merits were very low and simulated networks were unrecoverable. As can be seen, a different threshold value can be found for the temporal, spectral, connectivity factors and they were estimated successfully after −5 dB SNR. Fig. A2. C) demonstrated the similarity merits against bandwidth. As can be seen, the widths of band have little effect on the separation.

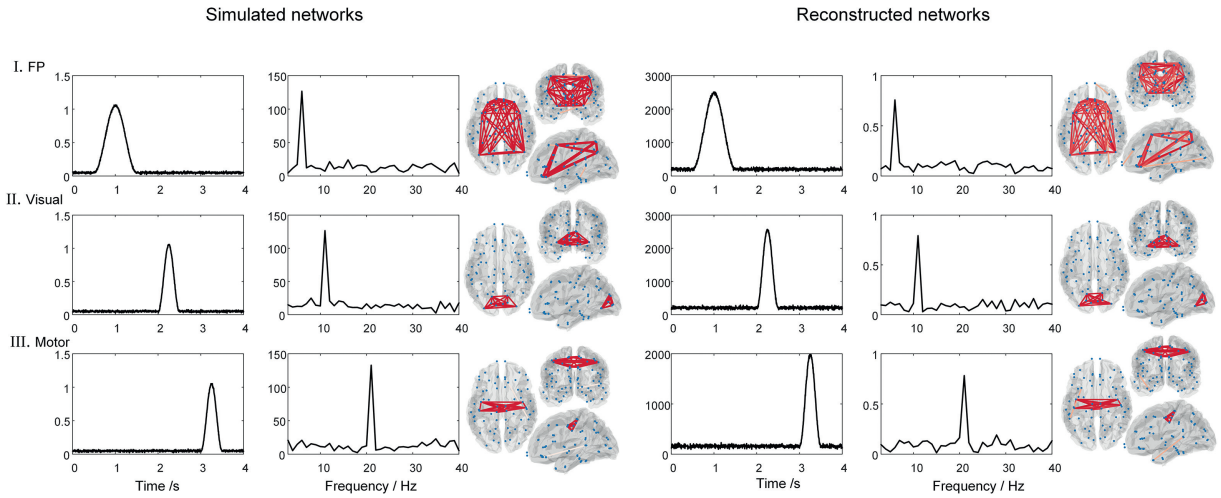

Fig. A1. Simulation results. Left: Simulated networks. Right: Reconstructed networks. Row I: Theta-oscillatory frontoparietal network forming in 1 s after onset. Row II: Alpha-oscillatory visual network forming around 2 s after stimuli onset. Row III: Beta-oscillatory network forming around 3 s after stimuli onset.

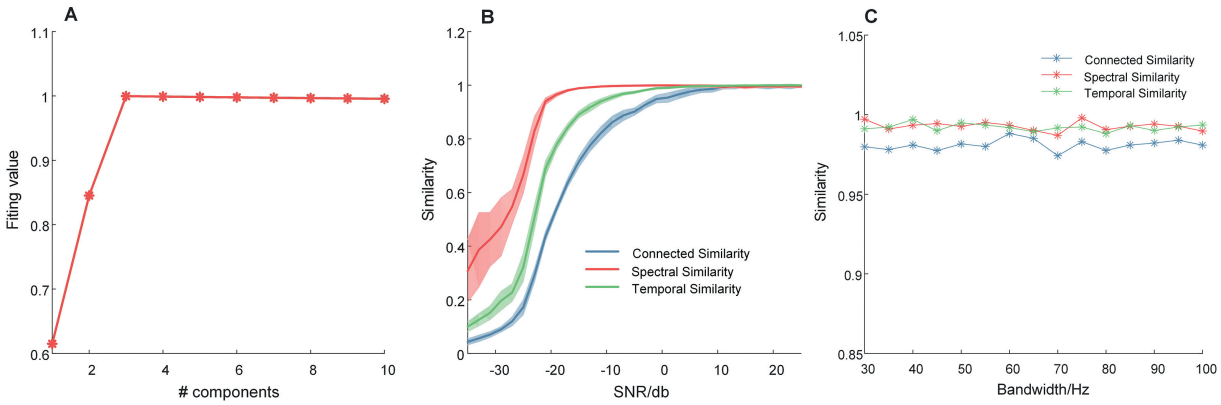

Fig. A2. A) Fit values as number of components. This plot unambiguously reveals J = 3 against the true number of components in the simulated data, in agreement with the ground truth. B) Similarity merits against SNR. As the SNR increases, similarity of three factors becomes higher and higher. After around −5 dB SNR, they can be reconstructed from data with a high accuracy. C) The similarity merits against bandwidth.

References

Al-sharoa, E., Al-khassaweneh, M., Aviyente, S., 2018. Tensor based temporal and multilayer community detection for studying brain dynamics during resting state fMRI. IEEE (Inst. Electr. Electron. Eng.) Trans. Biomed. Eng. 66 (3), 695–709.

Babiloni, F., Cincotti, F., Babiloni, C., Carducci, F., Mattia, D., Astolfi, L., Cheng, J., 2005. Estimation of the cortical functional connectivity with the multimodal integration of high-resolution EEG and fMRI data by directed transfer function. Neuroimage 24 (1), 118–131.

Bader, B.W., Kolda, T.G., 2012. Matlab Tensor Toolbox Version 2.5. Available online, January, 7.

Baker, A.P., Brookes, M.J., Rezek, I.A., Smith, S.M., Behrens, T., Smith, P.J.P., Woolrich, M., 2014. Fast transient networks in spontaneous human brain activity. eLife 3, e01867.

Barbey, A.K., Koenigs, M., Grafman, J., 2013. Dorsolateral prefrontal contributions to human working memory. Cortex 49 (5), 1195–1205. https://doi.org/10.1016/j.cortex.2012.05.022.

Betti, V., Corbetta, M., de Pasquale, F., Wens, V., Della Penna, S., 2018. Topology of functional connectivity and hub dynamics in the beta band as temporal prior for natural vision in the human brain. J. Neurosci. 38 (15), 3858–3871.
Betti, V., Della Penna, S., de Pasquale, F., Mantini, D., Marzetti, L., Romani, G.L., Corbetta, M., 2013. Natural scenes viewing alters the dynamics of functional connectivity in the human brain. Neuron 79 (4), 782–797.
Betzel, R.F., Bassett, D.S., 2017. Multi-scale brain networks. Neuroimage 160, 73–83.
Betzel, R.F., Gu, S., Medaglia, J.D., Pasqualetti, F., Bassett, D.S., 2016. Optimally controlling the human connectome: the role of network topology. Sci. Rep. 6, 30770.
Bola, M., Sabel, B.A., 2015. Dynamic reorganization of brain functional networks during cognition. Neuroimage 114, 398–413.
Brookes, M.J., Liddle, E.B., Hale, J.R., Woolrich, M.W., Luckhoo, H., Liddle, P.F., Morris, P.G., 2012a. Task induced modulation of neural oscillations in electrophysiological brain networks. Neuroimage 63 (4), 1918–1930.
Brookes, M.J., O'Neill, G.C., Hall, E.L., Woolrich, M.W., Baker, A., Corner, S.P., Barnes, G.R., 2014. Measuring temporal, spectral and spatial changes in electrophysiological brain network connectivity. Neuroimage 91, 282–299.
Brookes, M.J., Woolrich, M.W., Barnes, G.R., 2012b. Measuring functional connectivity in MEG: a multivariate approach insensitive to linear source leakage. Neuroimage 63 (2), 910–920.
Buzsáki, G., Draguhn, A., 2004. Neuronal oscillations in cortical networks. Science 304 (5679), 1926–1929.
Cichocki, A., Mandic, D., De Lathauwer, L., Zhou, G., Zhao, Q., Caiafa, C., Phan, H.A., 2015. Tensor decompositions for signal processing applications: from two-way to multiway component analysis. IEEE Signal Process. Mag. 32 (2), 145–163.
Cohen, M.X., 2014. Analyzing Neural Time Series Data: Theory and Practice. MIT press.
Colclough, G.L., Woolrich, M.W., Tewarie, P., Brookes, M.J., Quinn, A.J., Smith, S.M., 2016. How reliable are MEG resting-state connectivity metrics? Neuroimage 138, 284–293.
Cong, F., Lin, Q.-H., Kuang, L.-D., Gong, X.-F., Astikainen, P., Ristaniemi, T., 2015. Tensor decomposition of EEG signals: a brief review. J. Neurosci. Methods 248, 59–69.
Cong, F., Phan, A.H., Astikainen, P., Zhao, Q., Wu, Q., Hietanen, J.K., Cichocki, A., 2013. Multi-domain feature extraction for small event-related potentials through nonnegative multi-way array decomposition from low dense array EEG. Int. J. Neural Syst. 23 (02), 1350006.
Cong, F., Phan, A.H., Zhao, Q., Huttunen-Scott, T., Kaartinen, J., Ristaniemi, T., Cichocki, A., 2012. Benefits of multi-domain feature of mismatch negativity extracted by non-negative tensor factorization from EEG collected by low-density array. Int. J. Neural Syst. 22 (06), 1250025.
de Pasquale, F., Della Penna, S., Snyder, A.Z., Marzetti, L., Pizzella, V., Romani, G.L., Corbetta, M., 2012. A cortical core for dynamic integration of functional networks in the resting human brain. Neuron 74 (4), 753–764.
de Pasquale, F., Della Penna, S., Sporns, O., Romani, G., Corbetta, M., 2016. A dynamic core network and global efficiency in the resting human brain. Cerebr. Cortex 26 (10), 4015–4033.
Desikan, R.S., Ségonne, F., Fischl, B., Quinn, B.T., Dickerson, B.C., Blacker, D., Albert, M.S., 2006. An automated labeling system for subdividing the human cerebral cortex on MRI scans into gyral based regions of interest. Neuroimage 31 (3), 968–980.
Dima, D.C., Perry, G., Messaritaki, E., Zhang, J., Singh, K.D., 2018. Spatiotemporal dynamics in human visual cortex rapidly encode the emotional content of faces. Hum. Brain Mapp. 39 (10), 3993–4006. https://doi.org/10.1002/hbm.24226.
Dugué, L., VanRullen, R., 2017. Transcranial magnetic stimulation reveals intrinsic perceptual and attentional rhythms. Front. Neurosci. 11, 154.
Dugué, L., Xue, A.M., Carrasco, M., 2017. Distinct perceptual rhythms for feature and conjunction searches. J. Vis. 17 (3), 22-22.
Elbich, D.B., Molenaar, P.C., Scherf, K.S., 2019. Evaluating the organizational structure and specificity of network topology within the face processing system. Hum. Brain Mapp. 40 (9), 2581–2595.
Embury, C.M., Wiesman, A.I., Proskovec, A.L., Mills, M.S., Heinrichs-Graham, E., Wang, Y.P., Wilson, T.W., 2019. Neural dynamics of verbal working memory processing in children and adolescents. NeuroImage 185, 191–197.
Engel, A.K., Gerloff, C., Hilgetag, C.C., Nolte, G., 2013. Intrinsic coupling modes: multiscale interactions in ongoing brain activity. Neuron 80 (4), 867–886.
Fries, P., 2005. A mechanism for cognitive dynamics: neuronal communication through neuronal coherence. Trends Cognit. Sci. 9 (10), 474–480.
Fries, P., 2015. Rhythms for cognition: communication through coherence. Neuron 88 (1), 220–235.
Heinrichs-Graham, E., Wilson, T.W., 2015. Spatiotemporal oscillatory dynamics during the encoding and maintenance phases of a visual working memory task. Cortex 69, 121–130. https://doi.org/10.1016/j.cortex.2015.04.022.
Hillebrand, A., Barnes, G.R., Bosboom, J.L., Berendse, H.W., Stam, C.J., 2012. Frequency-dependent functional connectivity within resting-state networks: an atlas-based MEG beamformer solution. Neuroimage 59 (4), 3909–3921.
Hipp, J.F., Hawellek, D.J., Corbetta, M., Siegel, M., Engel, A.K., 2012. Large-scale cortical correlation structure of spontaneous oscillatory activity. Nat. Neurosci. 15 (6), 884.
Hunyadi, B., Dupont, P., Van Paesschen, W., Van Huffel, S., 2017. Tensor decompositions and data fusion in epileptic electroencephalography and functional magnetic resonance imaging data. Wiley Interdiscipl. Rev.: Data Min. Knowl. Discov. 7 (1), e1197.
Jensen, O., Kaiser, J., Lachaux, J.-P., 2007. Human gamma-frequency oscillations associated with attention and memory. Trends Neurosci. 30 (7), 317–324.
Kanatsoulis, C.I., Sidiropoulos, N.D., Akçakaya, M., Fu, X., 2019. Regular sampling of tensor signals: theory and application to fMRI. In: Paper Presented at the ICASSP 2019-2019 IEEE International Conference on Acoustics, Speech and Signal Processing (ICASSP).
Khambhati, A.N., Kahn, A.E., Costantini, J., Ezzyat, Y., Solomon, E.A., Gross, R.E., Seger, S., 2019. Functional control of electrophysiological network architecture using direct neurostimulation in humans. Netw. Neurosci. 3 (3), 848–877.
Kolda, T.G., Bader, B.W., 2009. Tensor decompositions and applications. SIAM Rev. 51 (3), 455–500.
Kopell, N.J., Gritton, H.J., Whittington, M.A., Kramer, M.A., 2014. Beyond the connectome: the dynome. Neuron 83 (6), 1319–1328.
Lachaux, J.-P., Axmacher, N., Mormann, F., Halgren, E., Crone, N.E., 2012. High-frequency neural activity and human cognition: past, present and possible future of intracranial EEG research. Prog. Neurobiol. 98 (3), 279–301.
Lachaux, J.P., George, N., Tallon-Baudry, C., Martinerie, J., Hugueville, L., Minotti, L., Renault, B., 2005. The many faces of the gamma band response to complex visual stimuli. Neuroimage 25 (2), 491–501.
Lachaux, J.P., Rodriguez, E., Martinerie, J., Varela, F.J., 1999. Measuring phase synchrony in brain signals. Hum. Brain Mapp. 8 (4), 194–208.
Larson-Prior, L.J., Oostenveld, R., Della Penna, S., Michalareas, G., Prior, F., Babajani-Feremi, A., Stout, J., 2013. Adding dynamics to the Human Connectome Project with MEG. Neuroimage 80, 190–201.
Lin, F.H., Belliveau, J.W., Dale, A.M., Hämäläinen, M.S., 2006. Distributed current estimates using cortical orientation constraints. Hum. Brain Mapp. 27 (1), 1–13.
Liu, Y., Moser, J., Aviyente, S., 2014. Network community structure detection for directional neural networks inferred from multichannel multisubject EEG data. IEEE (Inst. Electr. Electron. Eng.) Trans. Biomed. Eng. 61 (7), 1919–1930.
Mackevicius, E.L., Bahle, A.H., Williams, A.H., Gu, S., Denisenko, N.I., Goldman, M.S., Fee, M.S., 2019. Unsupervised discovery of temporal sequences in high-dimensional datasets, with applications to neuroscience. eLife 8, e38471.
Mahyari, A.G., Aviyente, S., 2014. Identification of dynamic functional brain network states through tensor decomposition. In: Paper Presented at the 2014 IEEE International Conference on Acoustics, Speech and Signal Processing (ICASSP).
Mahyari, A.G., Zoltowski, D.M., Bernat, E.M., Aviyente, S., 2016. A tensor decomposition-based approach for detecting dynamic network states from EEG. IEEE (Inst. Electr. Electron. Eng.) Trans. Biomed. Eng. 64 (1), 225–237.
Maris, E., Oostenveld, R., 2007. Nonparametric statistical testing of EEG-and MEG-data. J. Neurosci. Methods 164 (1), 177–190.
Mørup, M., Hansen, L.K., 2009. Automatic relevance determination for multi-way models. J. Chemometr.: J. Chemometr. Soc. 23 (7-8), 352–363.
Mørup, M., Hansen, L.K., Herrmann, C.S., Parnas, J., Arnfred, S.M., 2006. Parallel factor analysis as an exploratory tool for wavelet transformed event-related EEG. Neuroimage 29 (3), 938–947.
O'Neill, G.C., Tewarie, P., Vidaurre, D., Liuzzi, L., Woolrich, M.W., Brookes, M.J., 2018. Dynamics of large-scale electrophysiological networks: a technical review. Neuroimage 180, 559–576.
O'Neill, G.C., Barratt, E.L., Hunt, B.A., Tewarie, P.K., Brookes, M.J., 2015. Measuring electrophysiological connectivity by power envelope correlation: a technical review on MEG methods. Phys. Med. Biol. 60 (21), R271.
O'Neill, G.C., Tewarie, P.K., Colclough, G.L., Gascoyne, L.E., Hunt, B.A., Morris, P.G., Brookes, M.J., 2017. Measurement of dynamic task related functional networks using MEG. NeuroImage 146, 667–678.
Oldfield, R.C., 1971. The assessment and analysis of handedness: the Edinburgh inventory. Neuropsychologia 9 (1), 97–113.
Ozdemir, A., Bernat, E.M., Aviyente, S., 2017. Recursive tensor subspace tracking for dynamic brain network analysis. IEEE Trans. Signal Inf. Process. Netw. 3 (4), 669–682.
Palva, J.M., Wang, S.H., Palva, S., Zhigalov, A., Monto, S., Brookes, M.J., Jerbi, K., 2018. Ghost interactions in MEG/EEG source space: a note of caution on inter-areal coupling measures. Neuroimage 173, 632–643.
Pester, B., Ligges, C., Leistritz, L., Witte, H., Schiecke, K., 2015. Advanced insights into functional brain connectivity by combining tensor decomposition and partial directed coherence. PloS One 10 (6).
Popov, T., Jensen, O., Schoffelen, J.M., 2018. Dorsal and ventral cortices are coupled by cross-frequency interactions during working memory. Neuroimage 178, 277–286. https://doi.org/10.1016/j.neuroimage.2018.05.054.
Quinn, A.J., Vidaurre, D., Abeysuriya, R., Becker, R., Nobre, A.C., Woolrich, M.W., 2018. Task-evoked dynamic network analysis through hidden markov modeling. Front. Neurosci. 12, 603.
Raghavachari, S., Lisman, J.E., Tully, M., Madsen, J.R., Bromfield, E., Kahana, M.J., 2006. Theta oscillations in human cortex during a working-memory task: evidence for local generators. J. Neurophysiol. 95 (3), 1630–1638.
Salinas, E., Sejnowski, T.J., 2001. Correlated neuronal activity and the flow of neural information. Nat. Rev. Neurosci. 2 (8), 539.
Samdin, S.B., Ting, C.-M., Ombao, H., Salleh, S.-H., 2016. A unified estimation framework for state-related changes in effective brain connectivity. IEEE (Inst. Electr. Electron. Eng.) Trans. Biomed. Eng. 64 (4), 844–858.
Schölvinck, M.L., Leopold, D.A., Brookes, M.J., Khader, P.H., 2013. The contribution of electrophysiology to functional connectivity mapping. Neuroimage 80, 297–306.
Seedat, Z.A., Quinn, A., Vidaurre, D., Liuzzi, L., Gascoyne, L.E., Hunt, B.A., Woolrich, M.W., 2020. The role of transient spectral 'bursts' in functional connectivity: A magnetoencephalography study. NeuroImage, 116537.
Senoussi, M., Moreland, J.C., Busch, N.A., Dugué, L., 2019. Attention explores space periodically at the theta frequency. J. Vis. 19 (5), 22-22.
Sidiropoulos, N.D., De Lathauwer, L., Fu, X., Huang, K., Papalexakis, E.E., Faloutsos, C., 2017. Tensor decomposition for signal processing and machine learning. IEEE Trans. Signal Process. 65 (13), 3551–3582.
Siegel, M., Donner, T.H., Engel, A.K., 2012. Spectral fingerprints of large-scale neuronal interactions. Nat. Rev. Neurosci. 13 (2), 121.

Spyrou, L., Parra, M., Escudero, J., 2019. Complex tensor factorization with PARAFAC2 for the estimation of brain connectivity from the EEG. IEEE Trans. Neural Syst. Rehabil. Eng. 27 (1), 1–12.
Tang, M., Lu, Y., Yang, L., 2019. Temporal-spatial patterns in dynamic functional brain network for self-paced hand movement. IEEE Trans. Neural Syst. Rehabil. Eng. 27 (4), 643–651.
Tewarie, P., Hunt, B.A., O'Neill, G.C., Byrne, A., Aquino, K., Bauer, M., Brookes, M.J., 2019a. Relationships between neuronal oscillatory amplitude and dynamic functional connectivity. Cerebr. Cortex 29 (6), 2668–2681.
Tewarie, P., Liuzzi, L., O'Neill, G.C., Quinn, A.J., Griffa, A., Woolrich, M.W., Brookes, M.J., 2019b. Tracking dynamic brain networks using high temporal resolution MEG measures of functional connectivity. Neuroimage 200, 38–50.
Thornton, M.A., Conway, A.R., 2013. Working memory for social information: chunking or domain-specific buffer? Neuroimage 70, 233–239.
Timmerman, M.E., Kiers, H.A., 2000. Three-mode principal components analysis: choosing the numbers of components and sensitivity to local optima. Br. J. Math. Stat. Psychol. 53 (1), 1–16.
Varela, F., Lachaux, J.-P., Rodriguez, E., Martinerie, J., 2001. The brainweb: phase synchronization and large-scale integration. Nat. Rev. Neurosci. 2 (4), 229.
Vervliet, N., Debals, O., De Lathauwer, L., 2016. Tensorlab 3.0—numerical optimization strategies for large-scale constrained and coupled matrix/tensor factorization. In: Paper Presented at the 2016 50th Asilomar Conference on Signals, Systems and Computers.
Vidaurre, D., Hunt, L.T., Quinn, A.J., Hunt, B.A., Brookes, M.J., Nobre, A.C., Woolrich, M.W., 2018. Spontaneous cortical activity transiently organises into frequency specific phase-coupling networks. Nat. Commun. 9 (1), 2987.
Vidaurre, D., Quinn, A.J., Baker, A.P., Dupret, D., Tejero-Cantero, A., Woolrich, M.W., 2016. Spectrally resolved fast transient brain states in electrophysiological data. Neuroimage 126, 81–95.
Vidaurre, D., Smith, S.M., Woolrich, M.W., 2017. Brain network dynamics are hierarchically organized in time. Proc. Natl. Acad. Sci. Unit. States Am. 114 (48), 12827–12832.
Vinck, M., Oostenveld, R., Van Wingerden, M., Battaglia, F., Pennartz, C.M., 2011. An improved index of phase-synchronization for electrophysiological data in the presence of volume-conduction, noise and sample-size bias. Neuroimage 55 (4), 1548–1565.
Wang, D., Zhu, Y., Ristaniemi, T., Cong, F., 2018. Extracting multi-mode ERP features using fifth-order nonnegative tensor decomposition. J. Neurosci. Methods 308, 240–247.
Wens, V., Bourguignon, M., Goldman, S., Marty, B., De Beeck, M.O., Clumeck, C., De Tiege, X., 2014. Inter-and intra-subject variability of neuromagnetic resting state networks. Brain topogr. 27 (5), 620–634.
Williams, A.H., Kim, T.H., Wang, F., Vyas, S., Ryu, S.I., Shenoy, K.V., Ganguli, S., 2018. Unsupervised discovery of demixed, low-dimensional neural dynamics across multiple timescales through tensor component analysis. Neuron 98 (6), 1099–1115.
Winkler, A.M., Ridgway, G.R., Webster, M.A., Smith, S.M., Nichols, T.E., 2014. Permutation inference for the general linear model. Neuroimage 92, 381–397.
Woodward, T.S., Feredoes, E., Metzak, P.D., Takane, Y., Manoach, D.S., 2013. Epoch-specific functional networks involved in working memory. Neuroimage 65, 529–539.
Yamashita, M., Kawato, M., Imamizu, H., 2015. Predicting learning plateau of working memory from whole-brain intrinsic network connectivity patterns. Sci. Rep. 5, 7622.
Zhou, G., Cichocki, A., 2012. Canonical polyadic decomposition based on a single mode blind source separation. IEEE Signal Process. Lett. 19 (8), 523–526.
Zhou, G., Cichocki, A., Zhao, Q., Xie, S., 2015. Efficient nonnegative tucker decompositions: algorithms and uniqueness. IEEE Trans. Image Process. 24 (12), 4990–5003.
Zhou, G., Zhao, Q., Zhang, Y., Adalı, T., Xie, S., Cichocki, A., 2016. Linked component analysis from matrices to high-order tensors: applications to biomedical data. Proc. IEEE 104 (2), 310–331.
Zhu, Y., Li, X., Ristaniemi, T., Cong, F., 2019a. Measuring the task induced oscillatory brain activity using tensor decomposition. In: Paper Presented at the ICASSP 2019-2019 IEEE International Conference on Acoustics, Speech and Signal Processing (ICASSP). IEEE, pp. 8593–8597.
Zhu, Y., Liu, J., Mathiak, K., Ristaniemi, T., Cong, F., 2019b. Deriving electrophysiological brain network connectivity via tensor component analysis during freely listening to music. IEEE Trans. Neural Syst. Rehabil. Eng. 28 (2), 409–418.